Journal of Physiology - Paris 105 (2011) 25–35

Contents lists available at SciVerse ScienceDirect

Journal of Physiology - Paris

journal homepage: www.elsevier.com/locate/jphysparis

Encoding/decoding of first and second order tactile afferents in a neurorobotic application

Luca Leonardo Bologna [a,*], Jérémie Pinoteau [a], Romain Brasselet [a,1], Marco Maggiali [b], Angelo Arleo [a]

[a] CNRS, University Pierre & Marie Curie, Laboratory of Neurobiology of Adaptive Processes, UMR 7102, 9 quai St. Bernard, 75005 Paris, France
[b] Department of Robotics, Brain and Cognitive Sciences, Italian Institute of Technology, via Morego, 30, 16163 Genova, Italy

ARTICLE INFO

Keywords:
Primary tactile afferents
Mechanoreceptors
Second order cuneate nucleus neurones
Braille reading
Context separation
Fine touch discrimination
Neural coding
Information theory
Neurorobotics

ABSTRACT

We present a neurorobotic framework to investigate tactile information processing at the early stages of the somatosensory pathway. We focus on spatiotemporal coding of first and second order responses to Braille stimulation, which offers a suitable protocol to investigate the neural bases of fine touch discrimination. First, we model Slow Adaptive type I fingertip mechanoreceptor responses to Braille characters sensed both statically and dynamically. We employ a network of spiking neurones to transduce analogue skin deformations into primary spike trains. Then, we model second order neurones in the cuneate nucleus (CN) of the brainstem to study how mechanoreceptor responses are possibly processed prior to their transmission to downstream central areas. In the model, the connectivity layout of mechanoreceptor-to-cuneate projections produces a sparse CN code. To characterise the reliability of neurotransmission we employ an information theoretical measure accounting for the metrical properties of spiking signals. Our results show that perfect discrimination of primary and secondary responses to a set of 26 Braille characters is achieved within 100 and 500 ms of stimulus onset, in static and dynamic conditions, respectively. Furthermore, clusters of responses to different stimuli are better separable after the CN processing. This finding holds for both statically and dynamically delivered stimuli. In the presented system, when sliding the artificial fingertip over a Braille line, a speed of 40 – 50 mm/s is optimal in terms of rapid and reliable character discrimination. This result is coherent with psychophysical observations reporting average reading speeds of 30 – 40 ± 5 mm/s adopted by expert Braille readers.

1. Introduction

Fine touch discrimination is mediated by rapid and reliable responses to stimuli sensed by fingertip mechanoreceptors (Johansson and Birznieks, 2004). Even simple object manipulation requires the ability to convey optimal accounts of tactile percepts to the central nervous system in order to adopt closed-loop control policies. More specifically, peripheral encoding/decoding mechanisms must produce faithful spatiotemporal representations of sensed stimuli and all subsequent stages of the ascending somatosensory pathway must transmit these codes to downstream structures as efficiently as possible.

Microneurography studies in humans demonstrated the precision and rapidity of primary afferent neurones (e.g. fingertip mechanoreceptors) in encoding fine tactile stimuli into perfectly discriminable spike train patterns (Johansson and Birznieks, 2004). Mechanoreceptors innervate the epidermis and discharge according to mechanical indentations of the fingertip skin. The spike latencies of mechanoreceptor responses convey information about contact parameters fast enough to account for the use of tactile signals in natural manipulation (Johansson and Birznieks, 2004; Johansson and Flanagan, 2009). Primary afferent signals are processed by second order neurones in the cuneate nucleus (CN) of the brainstem, which constitutes the main synaptic relay along the somatosensory pathway from the fingertip to the central nervous system. The functional link between first and second order neurones (i.e. mechanoreceptors and cuneate cells) has not been thoroughly investigated, and experimental and computational findings on how information is processed along this pathway are still lacking.

We propose a neurorobotic framework to study neural coding at the level of first and second order tactile afferents. The presented approach arises from a larger study on haptic perception, in which a robotic setup was used to investigate fine touch discrimination during Braille reading tasks (Fig. 1A and B). Here, we simulate skin indentation protocols in which Braille-like tactile stimuli are delivered statically and dynamically to an artificial touch sensor (Fig. 1C). We model deformation analogue values through a simulator mimicking

* Corresponding author. Tel.: +33 (0)1 44 27 21 33; fax: +33 (0)1 44 27 26 69.
E-mail addresses: luca.bologna@upmc.fr (L.L. Bologna), jeremie.pinoteau@snv.jussieu.fr (J. Pinoteau), romain.brasselet@tuebingen.mpg.de (R. Brasselet), marco.maggiali@iit.it (M. Maggiali), angelo.arleo@upmc.fr (A. Arleo).
[1] Present address: MPI for Biological Cybernetics, Dept. Logothetis, Spemannstraße 38, 72076 Tübingen, Germany.

0928-4257/$ - see front matter © 2011 Elsevier Ltd. All rights reserved.
doi:10.1016/j.jphysparis.2011.08.002

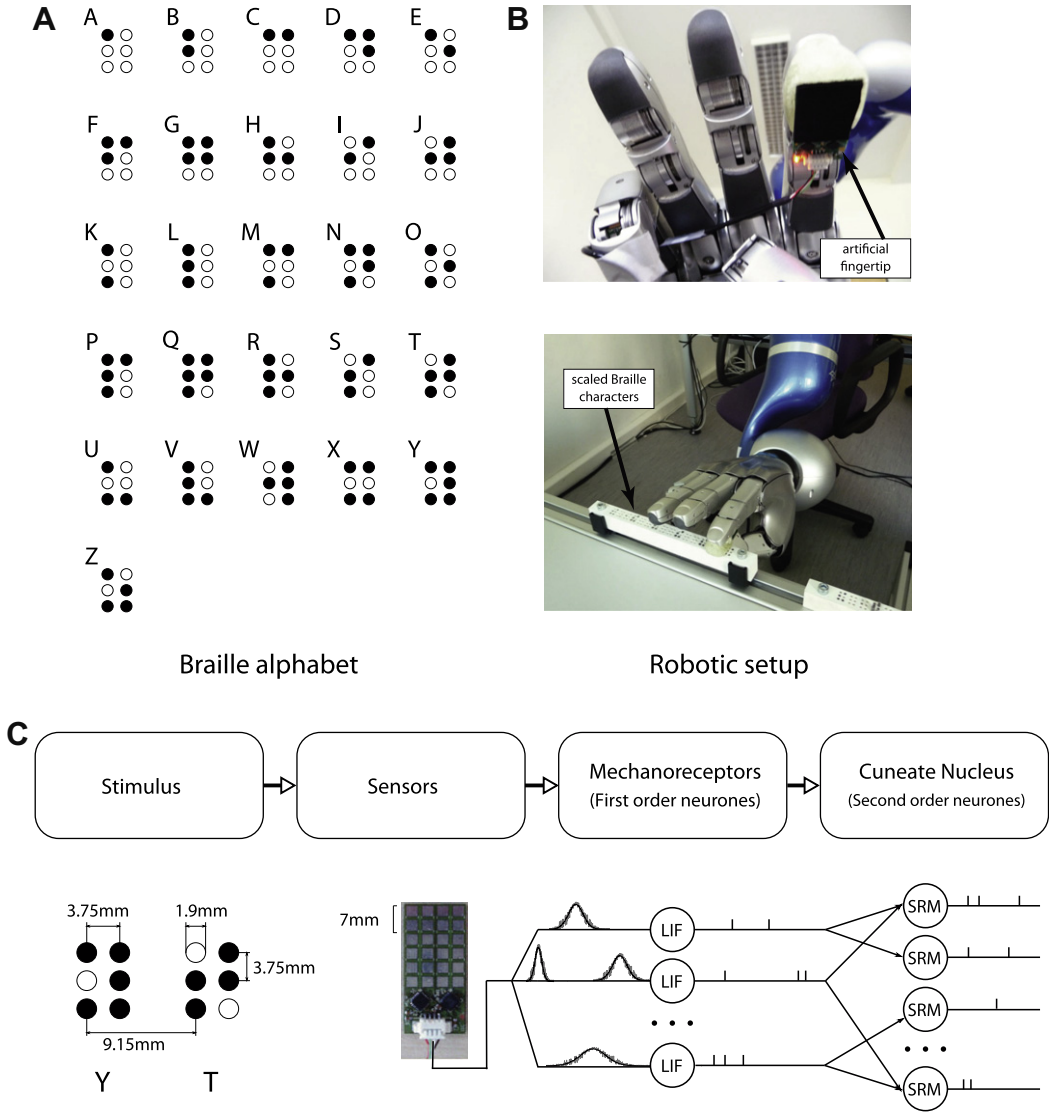

Fig. 1. *Overview of the robotic setup and entire encoding/decoding pathway.* (A) Braille alphabet. (B) The artificial fingertip mounted on a robotic hand/arm setup (© Institute of Robotics and Mechatronics, German Aerospace Center). (C) From left to right: we employ Braille-characters as tactile stimuli to indent a capacitive artificial touch sensor. The analogue responses provided by the touch sensor drive a network of Leaky-Integrate-and-Fire (LIF) neurones (Chacron et al., 2003) converting analogue signals into spiking activity and mimicking fingertip mechanoreceptors. The population of LIF neurones projects onto a network of Spike-Response-Model (SRM) units (Gerstner and Kistler, 2002) implementing second order cuneate nucleus (CN) cells of the brainstem.

skin indentation following orthogonal forces exertion. These analogue signals form the inputs to a network of leaky-integrate-and-fire neurones (LIF). The latter performs an analogue-to-spike conversion aiming at reproducing the activity of Slow Adapting type I (SA-I) mechanoreceptors in terms of both spiking discharge and receptive fields (see Johansson and Flanagan, 2009, for a recent review). The population of LIF neurones (i.e. simulated primary afferents) projects onto a network of second order units modelling CN neurones. We employ the Spike Response Model (SRM) (Gerstner and Kistler, 2002) to capture the stochastic nature of single cuneate responses (unpublished data by H. Jörntell). Drawing inspiration from our recent theoretical analysis of human microneurography recordings (Brasselet et al., 2011), we use a metrical information measure to estimate the amount of information transmitted by first and second order neurones about tactile stimulation. The same information measure quantifies stimulus separability at both stages of the considered pathway. The presented system succeeds in reconstructing both statically and dynamically delivered Braille-like stimuli rapidly and reliably. Also, the CN sparse re-encoding of primary afferent signals facilitates downstream discrimination of tactile stimuli and minimises destructive interference between similar percepts sensed by the artificial fingertip.

2. Material and methods

Fig. 1 shows the robotic setup used for the Braille scanning task and illustrates an overview of the considered encoding/decoding pathway. We adopt different experimental protocols in order to characterise neural coding at each processing stage (i.e. upstream and downstream from the cuneate nucleus network) and investigate fine touch discrimination. For the static stimulation protocols, we employ a set of 26 different probes reproducing a scaled version (1:1.67) of all Braille characters and we simulate orthogonal indentation on the fingertip skin. Following an experimental protocol used for microneurography recordings in humans (Johansson and Birznieks, 2004), we take a protraction phase of force application of 125 ms, a plateau phase of 250 ms, and a retraction phase of 125 ms. For the dynamic stimulation protocols, we rub the same probe set of Braille-characters over the simulated fingertip at different constant velocities, from 5 to 90 mm/s.

2.1. The artificial touch sensor

First, we employed an artificial skin prototype[2] (Cannata et al., 2008; Bologna et al., 2010) to collect and characterise a dataset of analogue responses to Braille-character tactile indentations. The entire artificial fingertip has a sensitive surface of approximately 18×23 mm. It consists of 24 capacitive square sensors disposed according to a rectangular grid layout. The dimension of each sensor is approximately of 3 mm and the inter-centre distance is 4 mm (Fig. 1C). The array is covered by a 2.5 mm thick neoprene layer in order to modulate the pressure exerted on the sensors. The higher the indentation of a conductive material on the neoprene, the stronger the response of the touch sensors. The response strength of each sensor ranges between 0 and 189 femtoFarads (fF). The acquisition frequency of the capacitive sensor is 20 Hz.

Second, we developed a simulator capable of reproducing the responses of the artificial fingertip, which allowed us to achieve a greater flexibility in data generation and higher acquisition frequencies (e.g. 1000 Hz). A previous study on the sensory device (Bologna et al., 2010) shows that a Gaussian kernel can fit its response. In Braille reading experiments, the touch sensor outputs varied between 0 and 60 fF and its receptive fields up to a 1.6 mm radius (depending on stimulation pattern). Therefore, we model the touch sensor response by means of a Gaussian kernel of amplitude 55 fF and standard deviation 1.6 mm. Additionally, in order to better reproduce the output variability, we add a white noise to the amplitude of the response (2.5 fF) and to its standard deviation (0.1 mm). Furthermore, we model the position error of the experimental setup by adding a Gaussian noise centred on the position of each stimulus (standard deviation 0.1 mm).

2.2. Modelling primary afferent responses: analogue-to-spike transduction

We implement a network of leaky integrate-and-fire (LIF) neurones (Lapicque, 1907; Chacron et al., 2003) to convert analogue touch sensor outputs into spike train patterns (Fig. 1C). We map the capacitance values provided by the touch sensor (proportional to probe indentations) into current intensities $I(t)$ driving the LIF neurones by applying a multiplicative gain factor of -390 pA/fF (determined by comparing output LIF spike trains against recorded mechanoreceptor responses, Johansson and Birznieks, 2004).

The dynamics of the membrane potential $V(t)$ of each LIF neuron is:

$$C \cdot \frac{dV(t)}{dt} = -g \cdot (V(t) - V_{leak}) - I(t) \tag{1}$$

where $C = 0.5$ nF denotes the membrane capacitance, $g = 25$ nS the passive conductance, $V_{leak} = -70$ mV the resting membrane potential, and $I(t)$ the total synaptic input of a neurone. The membrane time constant is then $\tau = C/g = 20$ ms. Whenever the membrane potential $V(t)$ reaches the threshold $V_{thr} = -50$ mV the LIF neurone emits an action potential. Then, its membrane potential is reset to $V_{reset} = -100$ mV and the dynamics of $V(t)$ is frozen during a refractory period $\Delta t_{ref} = 2$ ms. We also use a "threshold fatigue" (Chacron et al., 2003) to model the phenomenon of "habituation". It consists in increasing the threshold V_{thr} by a value A_{thr} each time the neurone discharges, making it harder for the neurone to spike again (i.e. preventing it from responding highly tonically even in the presence of strong inputs). In the absence of spikes, the threshold decreases exponentially back to its resting value $V_{restThr}$:

$$\frac{dV_{thr}(t)}{dt} = -\frac{V_{thr}(t) - V_{restThr}}{\tau_{thr}} \tag{2}$$

with $\tau_{thr} = 100$ ms, $V_{restThr} = -50$ mV and $A_{thr} = 50$ mV. We integrate Eqs. (1) and (2) using Runge–Kutta 2 and a timestep of 1 ms.

We consider networks of 6 and 12 LIF neurones, following the number of stimulated capacitive sensors (Fig. 2A), for the static and dynamic stimulation protocols, respectively. Fig. 2C and D show examples of mechanoreceptor spiking activity for both protocols.

2.3. Modelling second order neurones in the cuneate nucleus

We model single cuneate responses by means of the spike-response model (SRM) (Gerstner and Kistler, 2002) (see Brasselet et al., 2009, for a previous use of the model). We include a noise model (i.e. escape noise) that follows a stochastic process, so providing a linear probabilistic neuronal model. Thanks to its properties, the adopted SRM permits a higher transparency and controllability of all free parameters (e.g. synaptic integration time constant, amplitude and shape of excitatory post-synaptic potential).

An input spike arrival at time t induces a membrane potential depolarisation $\Delta V(t)$ described by:

$$\Delta V(t) \propto \sqrt{t} \exp(-t/\tau) \tag{3}$$

where the parameter $\tau = 3$ ms determines the decay time constant of the EPSP (excitatory postsynaptic potential). If several afferent spikes excite the neurone within a short time window, then the EPSPs adds linearly:

$$V(t) = V_r + \sum_{i,j} w_i \Delta V\left(t - \hat{t}_i^j\right) \tag{4}$$

where i denotes presynaptic neurones, j indexes the spikes emitted by a presynaptic neurone i at times $\hat{t}_i^j$, and $V_r = -70$ mV is the resting potential. The term w_i indicates the synaptic weight of the projection from the presynaptic unit i, defined as:

$$w_i = W \cdot w_i^{0,1} \tag{5}$$

with factor W determining the upper bound of the synaptic efficacy, and $w_i^{0,1}$ being constrained within the range [0,1]. We use $W = 1$ in our simulations. At each time step, a function $g(t)$ computes the instantaneous firing rate of the cell according to:

$$g(t) = r_0 \log\left(1 + \exp\left(\frac{V(t) - V_0}{V_f}\right)\right) \tag{6}$$

where the constants $r_0 = 0.01$ Hz, $V_0 = -66$ mV, $V_f = 1$ mV are the instantaneous firing rate, the probabilistic threshold potential, and a gain factor, respectively. A function $A(t)$ determines the refractoriness property of the neurone:

$$A(t) = \frac{(t - \hat{t} - \tau_{abs})^2}{\tau_{rel}^2 + (t - \hat{t} - \tau_{abs})^2} \mathcal{H}(t - \hat{t} - \tau_{abs}) \tag{7}$$

where $\tau_{abs} = 3$ ms and $\tau_{rel} = 1$ ms denote the absolute and relative refractory periods, respectively, $\hat{t}$ the time of the last spike emitted, and $\mathcal{H}$ the Heaviside function. Finally, the functions $g(t)$ and $A(t)$ allow the probability of firing $p(t)$ to be computed:

$$p(t) = 1 - \exp(-g(t)A(t)) \tag{8}$$

We implement the synaptic connections between mechanoreceptors and CN neurones so as to generate the receptive fields shown in Fig. 2B. Each CN neurone receives non-plastic inputs from either one or a group of two/three adjacent mechanoreceptors depending on the stimulation protocol (see the caption of Fig. 2 for details). The dimension and shape of the receptive fields and synaptic connection strength allow topographical information to be maintained at the level of the second order output space. Also, thanks to the adopted connectivity layout, CN neurones collecting signals from

[2] Developed at the Italian Institute of Technology (IIT), Genoa, Italy.

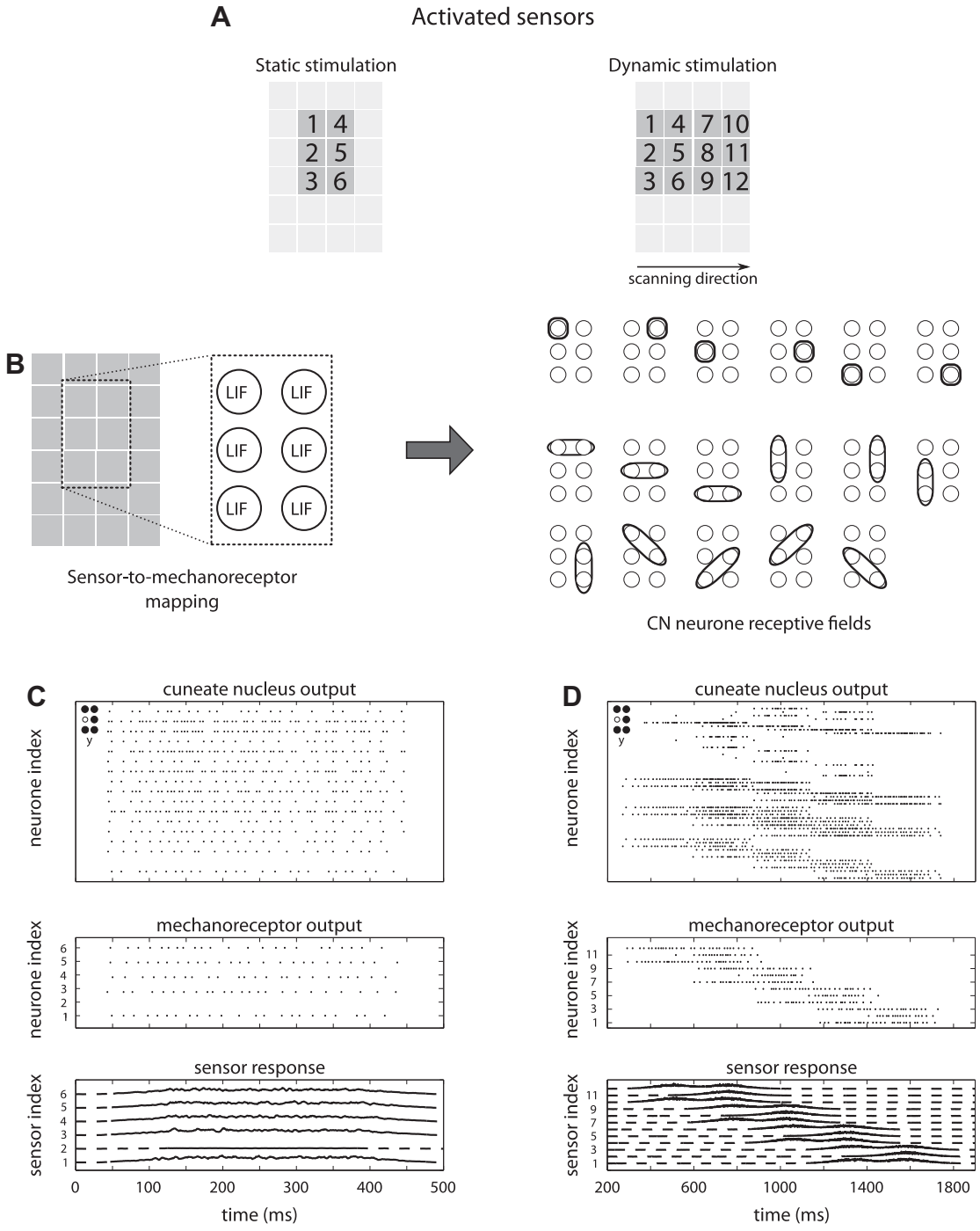

Fig. 2. *Network connectivity and examples of spike pattern responses.* (A) Touch sensor groups active during static (left) and dynamic (right) stimulation protocols. (B) LIF neurones modelling mechanoreceptor activity fulfil a topological mapping of fingertip regions (left). CN cell receptive fields are built so to collect activity of either a single cell or all possible pairs of adjacent mechanoreceptors, for the static stimulation protocol (right). Connectivity strength is set to 1. The same receptive fields are used in the dynamic protocol scenario, where CN cells responding to fingertip regions populated by three adjacent mechanoreceptors are also simulated (synaptic strength is either 1 or 0.7). (C) Example of sensor responses to a statically delivered stimulus "y" (bottom), mechanoreceptor activity during the entire stimulation period (centre) and corresponding CN encoding of first afferent output (top). Given to the aforementioned topographical mapping, neurone indices shown in the central plot correspond to sensor indices indicated in panel (A) (left) and in the bottom plot. Differently, no topographical mapping is present for cuneate cells, so we omitted any indexing for the sake of clarity. (D) same as (C) for a dynamically delivered stimulation (the same stimulus as (C) is used). Note how the temporal order of activation of the sensors (and neurones) depends on the character scanning direction (cf. panel (A)).

large receptive fields mirror both single primary neurone activation and multiple co-activations, so enriching the population spiking dynamics. Fig. 2C and D provide examples of touch sensor responses and corresponding mechanoreceptor and cuneate activities. We use populations of 17 and 49 neurones to simulate cuneate networks for static and dynamic stimulation, respectively.

2.4. Assessing neurotransmission reliability: metrical information analysis

Shannon mutual information (Shannon, 1948; Rieke et al., 1997) measures the interdependence between neural responses $r \in R$ and stimuli $s \in S$, treated as stochastic variables:

$$I(R;S) = \sum_s \sum_r p(r,s) \log \frac{p(r,s)}{p(r)p(s)} \quad (9)$$

where $p(s)$ and $p(r)$ are the marginal probabilities of stimulus and response, respectively, and $p(r,s)$ their joint probability.

In order to decode neural activities and quantify fine touch discrimination, we applied the recently defined metrical mutual information $I^*(R;S)$ (Brasselet et al., 2011). This information measure takes into account the metrical properties of the spike train space (Victor and Purpura, 1996; Schreiber et al., 2003; Van Rossum, 2001) and it has been proven to be suitable to decode the responses of human mechanoreceptors obtained via microneurography recordings (Brasselet et al., 2009, 2011). The definition of $I^*(R;S)$ relies on a similarity function based on the distance between spike train responses elicited by the same stimulus and by different stimuli. Here, we use the Victor-Purpura (VP) spike train metrics (Victor and Purpura, 1996) to compute the distance between two responses $r,r' \in R$, i.e. $D_{VP}(r,r')$. At each time point, we compute the distances between all spike trains up to that time point to assess metrical information and entropy over time (see below). In order to extend this metrics for population coding, we simply sum individual spike train distances to obtain the distance between two populations of spike trains.

The metrical mutual information is the difference between marginal and conditional metrical entropies (Brasselet et al., 2011):

$$I^*(R;S) = H^*(R) - H^*(R|S) \quad (10)$$

The marginal entropy $H^*(r)$ is:

$$H^*(R) = -\sum_{r\in R} \frac{1}{|R|} \log \sum_{r'\in R} \frac{\langle r|r'\rangle}{|R|} \quad (11)$$

where $\langle r|r'\rangle$ is the similarity measure between two population responses r and r' based on the spike train distance $D_{VP}(r,r')$; $|R|$ is the cardinal of the response space. The metrical conditional entropy $H^*(R|S)$ is defined as:

$$H^*(R|S) = \sum_{s\in S} p(s) H^*(R|s) \quad (12)$$

$$= -\sum_{s\in S} p(s) \sum_{r\in R_s} \frac{1}{|R_s|} \log \sum_{r'\in R_s} \frac{\langle r|r'\rangle}{|R_s|} \quad (13)$$

Here, we simply take the similarity measure $\langle r|r'\rangle$ as:

$$\langle r|r'\rangle = \mathcal{H}(D_{\text{critic}} - D_{VP}(r,r')) \quad (14)$$

where the critical distance D_{critic} is the cutoff parameter, and $\mathcal{H}$ the Heaviside step function. According to Eq. (14), as long as $D_{VP}(r,r') < D_{critic}$ the responses r,r' are considered as identical, otherwise they are considered as different. As reported previously (Brasselet et al., 2011), we set the optimal parameter D_{critic} by considering two sets of $D_{VP}(r,r')$ distances:

- the distances between the responses elicited by the same stimulus (named *intrastimulus* distances);
- the distances between the responses elicited by different stimuli (named *interstimulus* distances).

The optimality condition corresponds to maximum $I^*(R;S)$ and zero $H^*(R|S)$ and it occurs when the maximum intrastimulus distance—i.e. the size of the largest cluster of responses—becomes smaller than the minimum interstimulus distance—the smallest distance between clusters of responses (Brasselet et al., 2011). In the case of neurotransmission, the relationship between intra- and interstimulus distance distributions tends to evolve over time as the input spike waves across multiple afferents flow in the readout system. Thus, the optimality condition is met when the distributions of intra- and interstimulus distances stop overlapping. The critical parameter D_{critic} is then taken as the maximal intrastimulus distance at the time when it becomes smaller than the minimum interstimulus distance. The time at which D_{critic} can be determined indicates when perfect input discrimination is achieved.

3. Results

3.1. Characterisation of mechanoreceptor responses

Fig. 3 compares some characteristics of simulated and human mechanoreceptor responses (Phillips et al., 1990; Johansson and Birznieks, 2004) when applying Braille-character probes to indent the fingertip skin. Fig. 3A focuses on receptive fields and shows some examples of Fast Adaptive type I (FA-I), Slow Adaptive I (SA-I), and simulated mechanoreceptor recordings upon stimulation with Braille characters. Both FA-I and SA-I primary afferents show a topological mapping (i.e. their activity correlates with the area of stimulation), demonstrating their role in encoding spatial discontinuities (Johansson and Flanagan, 2009). There is no clear experimental evidence on whether SA-I or FA-I mechanoreceptors primarily carry the information needed for Braille character recognition (Phillips et al., 1990). Nonetheless, the receptive fields of SA-I afferents seem to reproduce Braille spatial patterns with higher accuracy than FA-I (see Fig. 3A, top). Our simulated primary afferent responses exhibit receptive fields qualitatively similar to those of real SA-I units, in terms of shape, dimensions and signal-to-noise ratio (Fig. 3A, bottom).

Fig. 3B compares the first spike jitter of model primary responses against that of their biological counterparts (SA-I units). The two distributions of Fig. 3B appear to be statistically equivalent (Mann–Whitney U test $P > 0.11$; Kolmogorov–Smirnov test $P > 0.076$) in terms of both median and shape, despite a time lag of about 2 ms. Thus, modelled mechanoreceptors present the same variability in spike latencies as SA-I afferents, but on a larger time scale. We then compare the inter-spike interval (ISI) distributions (Fig. 3C) and find that spike trains of model neurones lack the ISI variability of those recorded in humans (although a Mann–Whitney U test shows that both distribution medians are equivalent, $P > 0.16$). The difference in ISI variability may be due to the viscoelastic properties and more complex dynamics of the human skin as compared to the artificial finger.

3.2. Information content of primary afferent responses

We perform an information theoretical analysis to decode simulated first order responses to 26 distinct Braille characters sensed both statically and dynamically (Figs. 4 and 5, respectively). We focus on the evolution of information over time and quantify how rapidly perfect discrimination of all Braille stimuli can be achieved after stimulus onset.

3.3. Decoding primary afferent responses to static Braille stimuli

Fig. 4A top illustrates the evolution of maximal and minimal inter- and maximal intrastimulus distances over time (continuous and dashed lines, respectively) upon *static* indentation of Braille stimuli. Within 100 ms of the stimulus onset the maximum intrastimulus distance becomes smaller than the minimum interstimulus distance so satisfying the condition for an errorless stimulus reconstruction—i.e. maximal metrical information $I^*(R;S)$ and zero conditional entropy $H^*(R|S)$, as shown in Fig. 4B. Consistent to previous decoding analysis on real primary afferent recordings (Johansson and Birznieks, 2004), such a fast and complete discrimination occurs before the end of the indentation protraction phase (Fig. 4A, centre), which corresponds to the period of strongest and best timed spiking responses of simulated mechanoreceptors (see the sample PSTH of Fig. 4A, bottom).

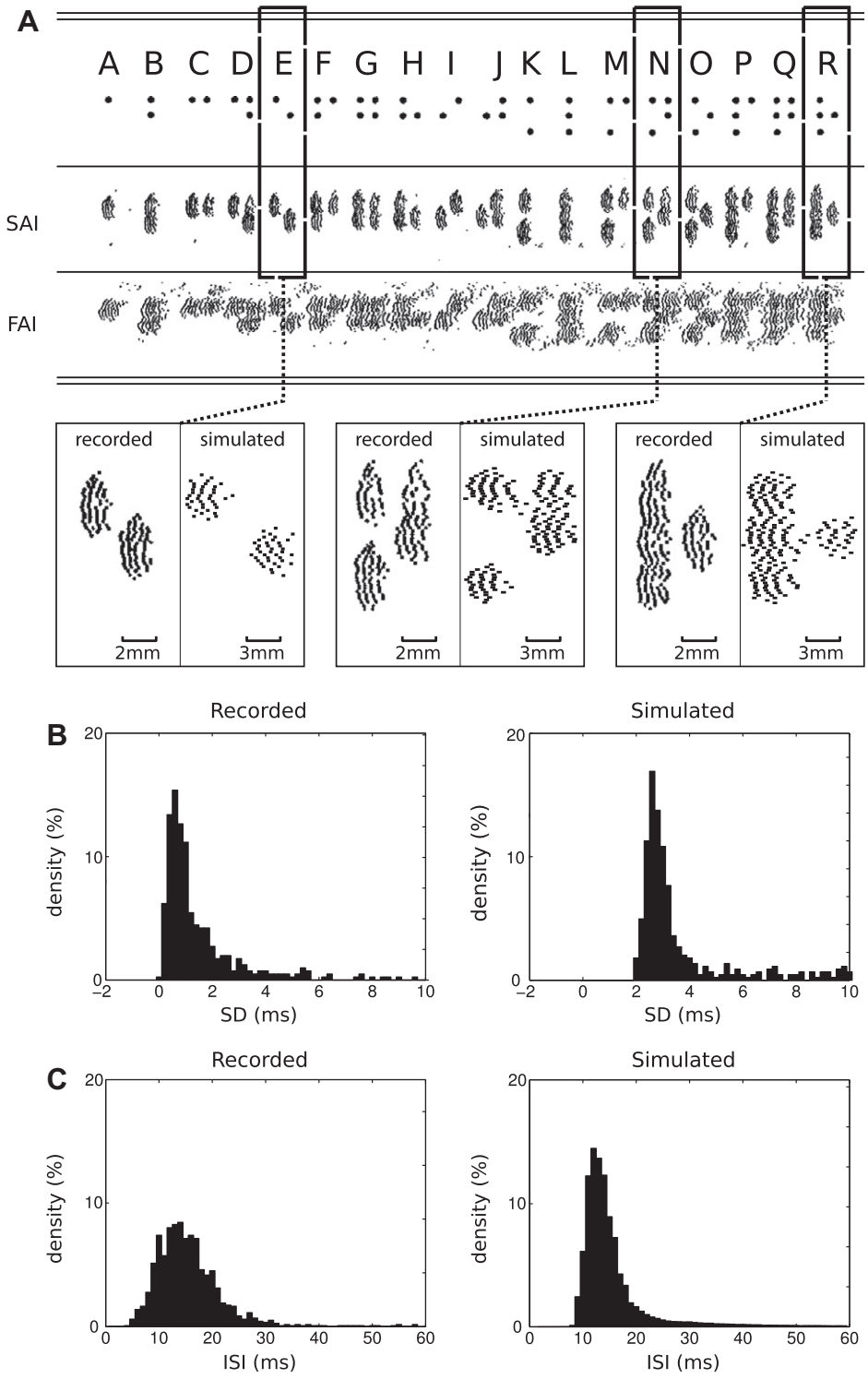

Fig. 3. *Characterisation of mechanoreceptor responses.* (A) Top: Spatial event plots of human mechanoreceptor responses to scanned Braille characters 'a' to 'r' (top, adapted from Phillips et al., 1990). Bottom: Zoomed in sections comparing the receptive field of three SA-I mechanoreceptors against those of their simulated counterparts. (B) Distribution of standard deviations (SD) of first-spike latencies for both SA-I (left) and simulated (right) mechanoreceptor responses to comparable stimuli. (C) Distribution of inter-spike intervals (ISIs) for both SA-I (left) and simulated (right) mechanoreceptor responses. In (B) and (C), the recorded distributions are reconstructed from data by Johansson and Birznieks (2004). In both cases, data are pooled across different stimulus directions and afferents.

Fig. 4C reports two examples of matrices of spike train distances between simulated mechanoreceptor responses before (left) and after (right) the occurrence of the perfect discrimination condition (i.e. at $t \approx 100$ ms). For $t < 100$ ms (left matrix) responses to different stimuli can have relatively small distances, which produces interferences impairing the decoding process. By contrast, for $t > 100$ ms (right matrix) all the initially overlapping contexts become well separated, removing all interferences across inputs and leading to 100% accuracy in the discrimination process. Note the different colormap scales used to represent spike train distances D_{VP} before and after the occurrence of the optimality condition.

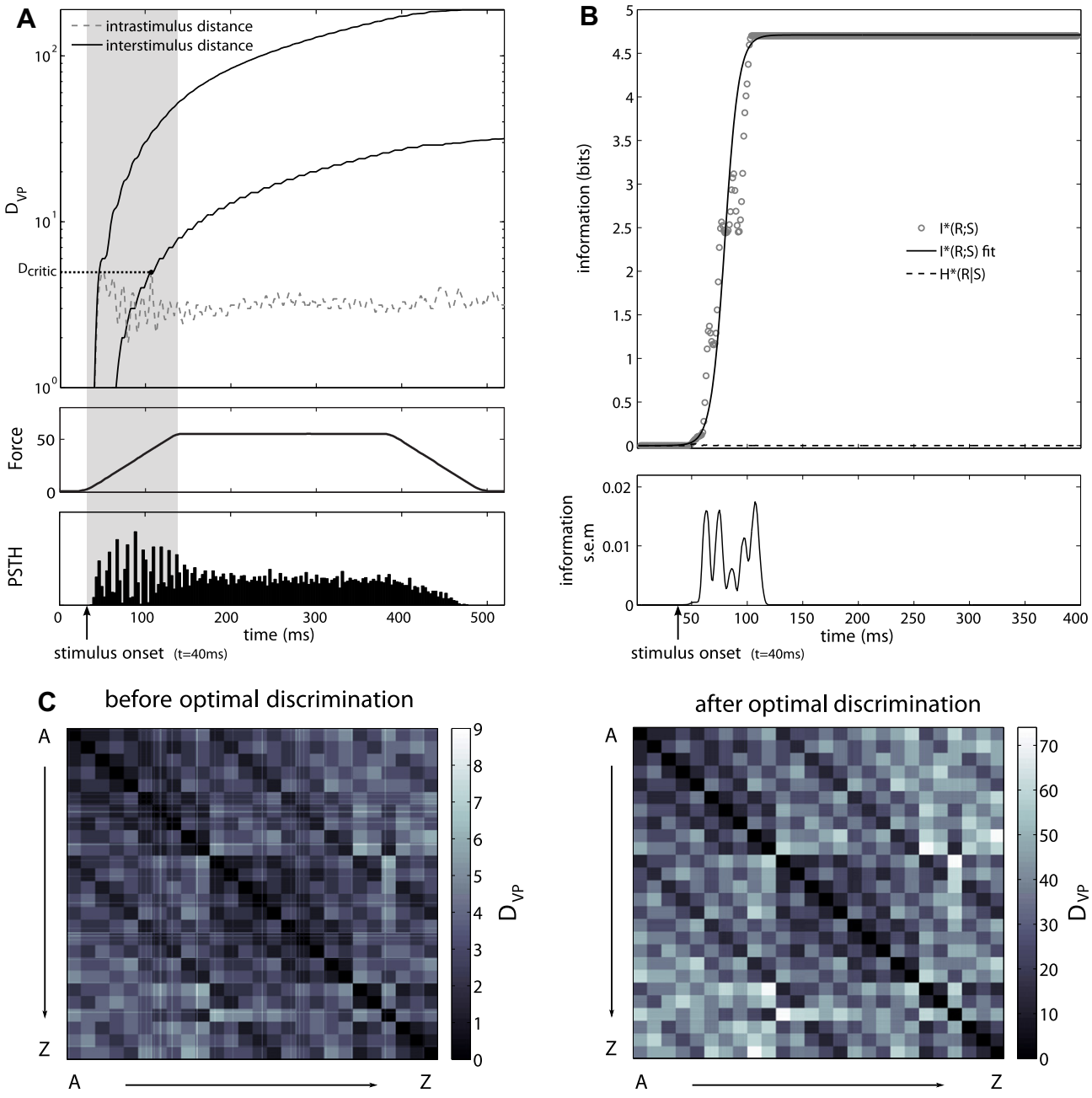

Fig. 4. *Decoding analysis of primary afferent responses to static Braille stimuli.* (A) Top: Evolution of maximal and minimal interstimulus and maximal intrastimulus distance over time (continuous and dashed curves respectively) on a semilogarithmic scale. The minimal intrastimulus distance is approximately zero during the entire stimulus duration and has not been reported. Twenty repetitions per stimulus are used. Perfect discrimination—occurring when the maximum intrastimulus distance becomes smaller than the minimum interstimulus distance—is achieved within about 100 ms of stimulus onset. The critical distance used for computing the metrical information and entropy is indicated by D_{critic}. Centre: Time course of the stimulus indentation force shows that the perfect discrimination is reached well before the end of the protraction phase ($t < 125$ ms). Bottom: The Post Stimulus Time Histogram (PSTH) reveals a stronger activity during the protraction phase as observed for human SA-I type mechanoreceptors (Johansson and Flanagan, 2009). (B) Top: Metrical information (grey circles: data; continuous black line: sigmoidal fit) converges to its maximal value after about 100 ms, while the metrical conditional entropy (dashed black line) remains equal to zero. Bottom: information variability, measured as mean standard error (s.e.m), over time. (C) Distances between mechanoreceptor responses before (left matrix) and after (right matrix) the perfect discrimination condition is reached. Twenty repetitions for each character are used and distances computed between all of the 520^2 spike train pairs. Each line shows the distances between a single response to a stimulus and all other responses. Intrastimulus distances are grouped into small squares (20-sample side) along the diagonal and are remarkably smaller than the others (i.e. interstimulus distances) after optimal discrimination (right matrix).

3.4. Decoding primary afferent responses to dynamic Braille stimuli

In a second information theoretical analysis we consider simulated data obtained with *dynamically* delivered stimuli. As the fingertip scans a Braille character at a constant velocity of 15 mm/s, skin deformations generated by dot movements supply simulated mechanoreceptors with analogue spatiotemporal patterns changing over time. As expected, mechanoreceptors' spike train responses reflect these displacement patterns rather faithfully (see example of Fig. 2D).

Again, we investigate how maximal and minimal intra- and interstimulus distances evolve over time. Fig. 5A shows that the condition of perfect discrimination of 26 Braille inputs—dynamically delivered to the fingertip—is reached after about 700 ms from stimulus onset. As predicted by metrical information theory, this condition corresponds to maximum information

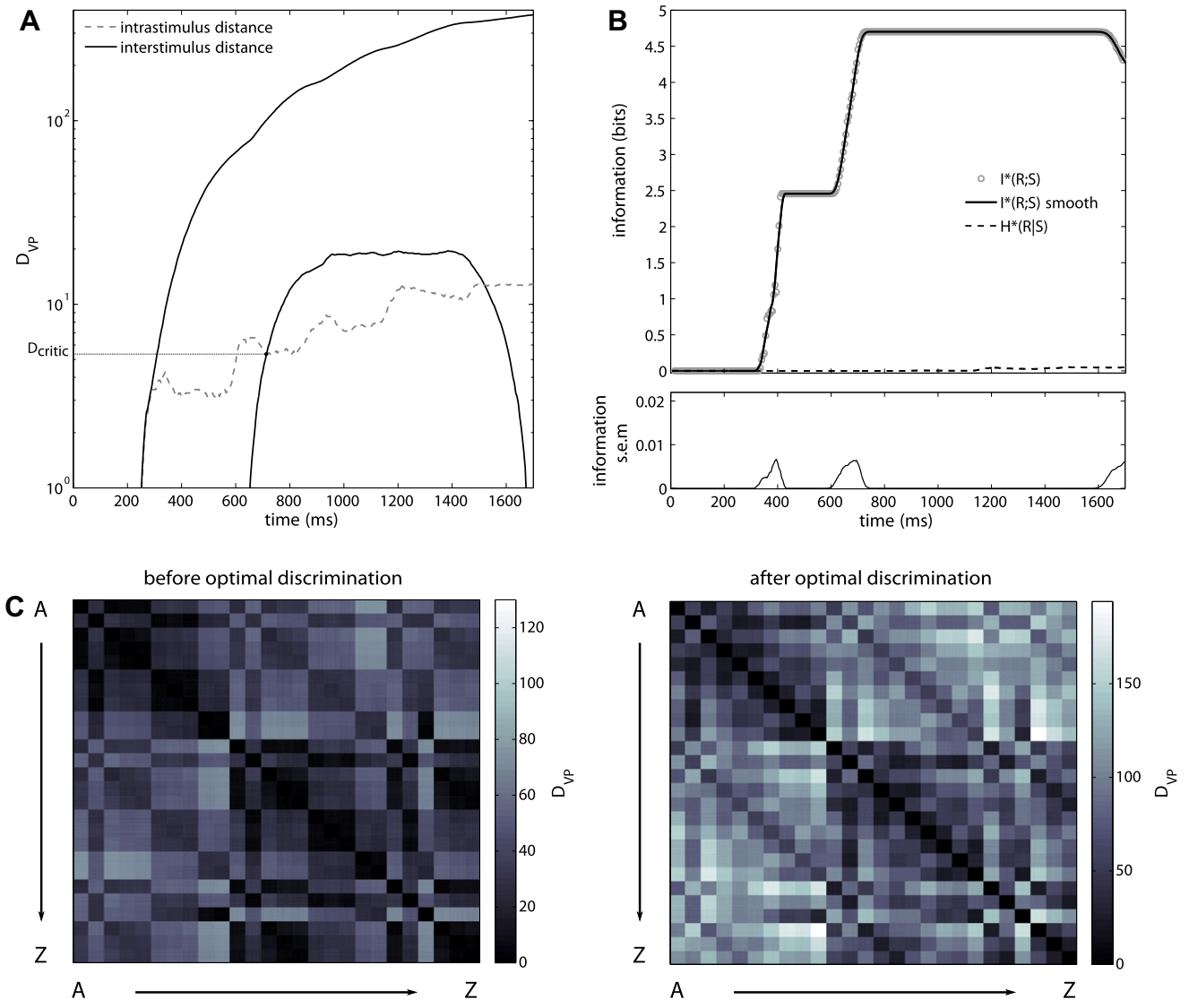

Fig. 5. *Decoding analysis of primary afferent responses to dynamic Braille stimuli.* (A) Evolution of maximal and minimal interstimulus and maximal intrastimulus distance over time (continuous and dashed curves respectively) on a semilogarithmic scale. The minimal intrastimulus distance is approximately zero during the entire stimulus duration and has not been reported. The critical distance used for computing the metrical information and entropy is indicated by D_{critic}. Sixty repetitions per stimulus are used. Perfect discrimination occurs after 700 ms from stimulus onset. Note that at the end of the stimulus application the minimum interstimulus distance becomes smaller than the maximum intrastimulus distance, meaning that interferences between similar stimuli impair the discrimination process. (B) Top: The time course of information (grey circles: data; continuous black line: sliding window smoothing) and of conditional entropy (dashed black line) confirms that perfect discrimination of all 26 Braille characters is achieved at time $t \approx 700$ ms. Bottom: information variability, measured as mean standard error (s.e.m), over time. (C) Matrices of response distances before (left) and after (right) perfect discrimination (see Fig. 4C legend for details on matrix entry values).

and zero conditional entropy (Fig. 5B). As expected, the metrical information curve (black line) exhibits a plateau starting at around 400 ms and lasting for about 120 ms. This corresponds to the stimulation phase during which the first column of Braille dots enters in contact with the fingertip while the second does not stimulate any sensor yet. The information value at plateau is about half of the total amount of information transmitted (Fig. 5B).

As for the static indentation scenario, the distance matrices between all mechanoreceptor responses (Fig. 5C) mirror the fulfilment of the optimality condition. In fact, while clusters of responses to different stimuli overlap at the beginning of the stimulation (left matrix), they are completely apart once the perfect context separation is achieved (right matrix). (Again, note the different colormap scales).

3.5. Information content of second order neurone responses

We then investigate how the processing mediated by the cuneate nucleus (CN) network can impact fine touch discrimination. We focus on both the time necessary to achieve complete discrimination and the efficiency in context separation downstream of the CN.

3.6. Decoding second order responses to static Braille stimuli

The metrical information analysis of CN response patterns elicited by *static* tactile stimulation shows that perfect discrimination of all Braille stimuli occurs approximately within 100 ms of stimulus onset (Fig. 6A) as for the primary afferent level (Fig. 4B). This result suggests that the chosen mechanoreceptor-to-CN

connectivity layout allows first order encoding efficacy to be maintained after neural processing at the CN stage. Again, as reported in Fig. 6A, the optimality condition corresponds to maximal information (continuous black line) and nil conditional entropy (dashed black line). The two distance matrices of Fig. 6C show qualitatively that input context separability can indeed be achieved significantly better after 100 ms of stimulus onset. (Again, note the different scales of the D_{VP} colormaps). For sake of comparison between first and second order encoding efficacy, we do not take into account the conduction delay necessary for peripheral action potentials to propagate along the median nerve and reach the CN—the mean conduction velocity along the median nerve is about 60 m/s (Vallbo and Johansson, 1984).

To measure context separability before and after processing at the CN stage we quantify the average separation between intrastimulus and interstimulus distance distributions at the end of skin indentation (i.e. after 500 ms of stimulus onset). The inset of Fig. 6B depicts two examples of intra- and interstimulus distance distributions upstream (top) and downstream (bottom) of the CN. The histograms of Fig. 6B quantifies the mean separation δ between the two distributions before and after the CN. This result suggests that the overall distances between spike response patterns increase significantly (Mann–Whitney U test, $P < 0.0001$) downstream of the CN, augmenting the separability of whichever pair of responses belonging to different clusters.

3.7. Context separation of dynamic Braille stimuli mediated by CN responses

Given the spatial arrangement of Braille dots and the homogeneous structure of the artificial touch sensor, different characters may lead to exactly the same mechanoreceptor responses, in terms of spike count, when rubbed over the fingertip. In fact, the scanning of symmetrical Braille letters ('e' and 'i', 'd' and 'f', 'h' and 'j', 'r' and 'w', see Fig. 1A) activates the same subgroup of fingertip sensors for the same amount of time. As a consequence, although an early correct discrimination occurs, the interference between those Braille patterns increases over time, which finally produces the same activity of first order (LIF) neurones. Here, we investigate whether the mapping of primary afferent signals onto a higher dimensional space operated by the model CN might be suitable to avoid these interferences. We perform a Principal Component Analysis (PCA) to visualise the separability of first and second order response clusters over time. Fig. 7 shows the results obtained by projecting the clusters of responses to letters 'e' and 'i' onto the space defined by the first two principal components. In the case of first order processing (Fig. 7A), patterns 'e' and 'i' are well separated at the beginning of the trial ($t = 300$ ms) due to the activation of different mechanoreceptors. However, as the fingertip proceeds over the probe, the two signals become less separated and finally overlap at the end of the trial ($t = 1500$ ms). This is confirmed by

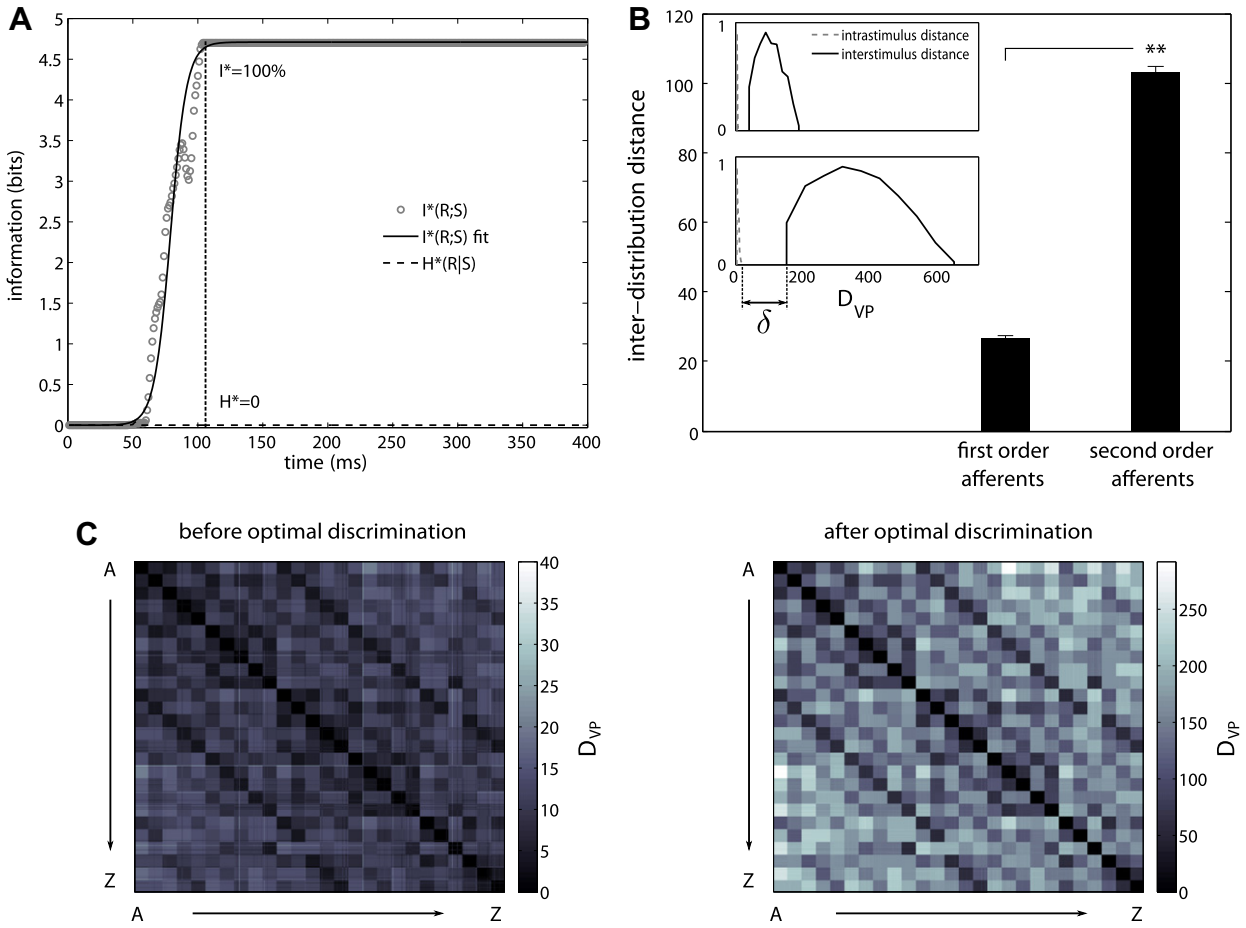

Fig. 6. *Decoding analysis of second order responses to static Braille stimuli.* (A) Perfect discrimination condition (i.e. $I^*(R;S) = 100\%$ and $H^*(R|S) = 0$) is reached after ≈ 100 ms from stimulus onset. (B) Average separation (δ) between intrastimulus and interstimulus distance distributions at the end of skin indentation (i.e. after 500 ms of stimulus onset). The separation is significantly larger downstream of the CN than at the level of mechanoreceptor outputs (Mann–Whitney U test, $P < 0.0001$). The inset shows an example of intra- and interstimulus distance distributions for mechanoreceptor (top) and CN (bottom) responses. (C) Distance matrices before (left) and after (right) the perfect discrimination condition is reached (see Fig. 4C legend for details on matrix entry values).

the decrease in information observed at the end of the scanning period shown in Fig. 5B. In fact, the metrical information value falls to about 4.219 which indicates that the decoder is able to discriminate at most 18 characters out of 26—i.e. the eight symmetric characters cannot be recognised anymore.

The same analysis on CN responses (Fig. 7B) shows that the initial distance between the two clusters augments with time providing an even better separation at the end of the trial. The mechanoreceptor-to-CN mapping is at the basis of the observed discrimination improvement. In fact, the chosen connectivity layout makes specific CN neurones respond to different mechanoreceptor co-activations. Hence, the following sparsification of the code guarantees a correct discrimination even at the end of the trial, with the n-dimensional CN response clusters becoming further apart.

3.8. Tactile discrimination efficacy as a function of Braille scanning velocity

We then compute, at the level of CN responses, the activity information content and discrimination time (i.e. time to converge to maximal information) as a function of 16 scanning velocities in the range 5 – 90 mm/s. Fig. 8A shows that for values between 5 – 50 mm/s, the time necessary to achieve maximum discrimination decreases exponentially. Within the same speed range, the information remains constant at its maximum value (indicating perfect discrimination of all Braille characters). For higher reading velocities, recognition time stabilises between 400 and 500 ms, but a significant reduction in information content occurs, making a complete stimulus discrimination impossible. These results show the existence of a trade-off between scanning speed and discrimination capabilities, with an optimal velocity range for single Braille character recognition of 40 – 50 mm/s (see also Fig. 8B).

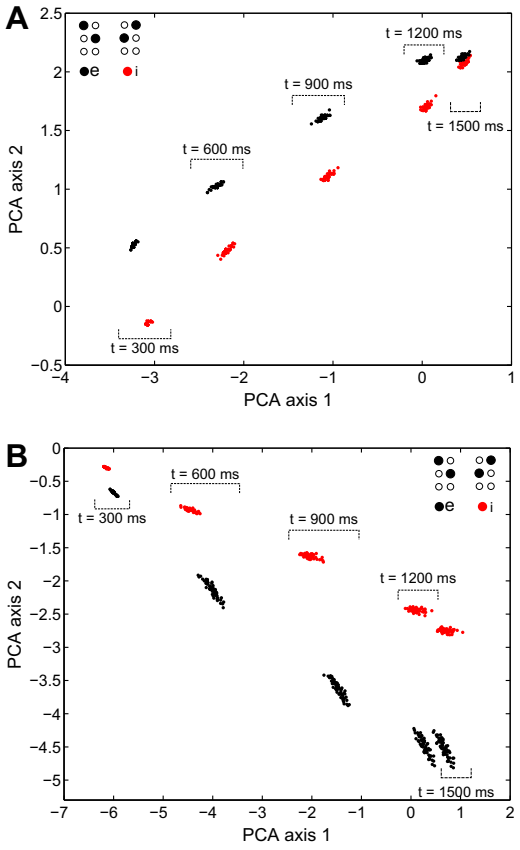

Fig. 7. *Context separation of dynamic Braille stimuli mediated by cuneate responses.* Principal component analysis (PCA) on responses to stimuli 'e' and 'i' upstream (A) and downstream (B) of the CN. PCA is applied to the matrices of individual neurone responses computed in terms of spike count at different times. At each considered time point, the entire spike trains up to that time point are taken into account. Clusters of responses projected on the two principal component axes have comparable distances at the beginning of the stimulation at both mechanoreceptor and CN neurone output (note that *x*-axis and *y*-axis scales are different). Nonetheless, the separation between clusters decreases over time for primary afferent responses (indicating higher interferences), whereas it increases at the level of second order neurones (denoting a better separability).

4. Discussion

Human microneurography studies have described the stimulus–response dynamics of fingertip mechanoreceptors and their electrophysiological properties under manifold stimulation conditions (Phillips et al., 1990, 1992; Johansson and Flanagan, 2009). These works showed that primary afferents are characterised by low variability in the response latency and highly informative spatiotemporal population activity. They also suggested that these properties allow a complete discrimination of a rich repertoire of different stimuli to be performed as soon as the first afferent spike wave is emitted (Johansson and Birznieks, 2004). Downstream from fingertip mechanoreceptors, second order neurones in the cuneate nucleus (CN) of the brainstem might be in charge of an efficient decoding and re-encoding of tactile signals. It has been proposed that the divergence/convergence ratio of the projections from primary afferents to CN neurones (Jones, 2000), together with the variability in afferent conduction velocity, can be relevant to the decoding of a large number of

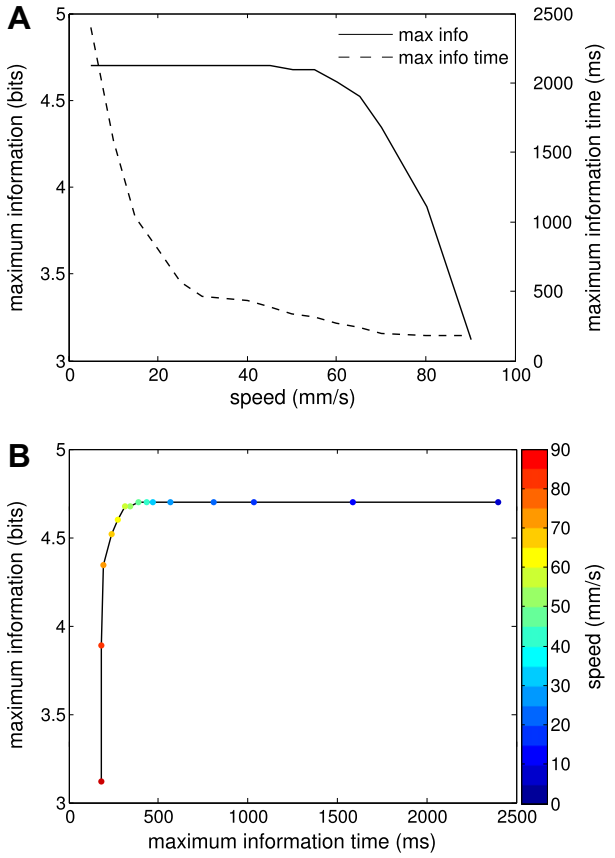

Fig. 8. *Tactile discrimination efficacy as a function of Braille scanning velocity.* (A) Maximal metrical information (solid line) and time necessary to reach maximum information (dashed line) plotted against scanning velocity. (B) Maximal information as a function of recognition time. Both diagrams show that the optimal velocity range in terms of scanning speed and discrimination accuracy is 40 – 50 mm/s.

stimuli and the conversion from temporal to spatial information by means of coincidence detection mechanisms (Johansson and Flanagan, 2009). Nonetheless, theoretical models exploring the role of second order CN neurones are still lacking and no hypothesis has been proposed concerning a CN role different from that of a synaptic relay (Canedo et al., 2000; Sánchez et al., 2003).

In this study we combine a neurorobotic approach—implementing first and second order tactile signal processing—with a metrical information theoretical analysis—based on distances in the spike train space—to study neural coding at the early stages of the haptic ascending pathway. We put forth the hypothesis that, in our system, CN neurones could perform a better stimulus separation than primary afferents. To test this hypothesis, we structure the network connectivity so that each CN cell responds according to a specific receptive field. We use the full set of Braille-alphabet letters to stimulate an artificial touch sensor both statically and dynamically. Our results demonstrate that, similar to primary afferents, the model CN activity allows a downstream decoder to perform a complete and fast input discrimination. Also, clusters of responses to different stimuli are more separable downstream from the CN than upstream. In the model, CN receptive fields work as a family of kernel functions projecting primary spike trains onto a higher dimensional space in which response clusters become farther apart. Furthermore, a principal component analysis shows that the context separation mediated by the CN under a dynamical stimulation scenario guarantees a better discrimination of input patterns creating response interferences at the level of primary afferents.

To explore the limits of the presented neurorobotic system with respect to character discrimination, we test its performance by scanning single Braille letters at different translational velocities. We find that a trade-off exists between discrimination capabilities and scanning speed. The optimal performance-velocity compromise occurs at around 40 to 50 mm/s. Provided that simulated Braille characters and mechanoreceptors are scaled up (1:1.67) with respect to real ones, our results are coherent with those observed on human Braille reading experiments (Mousty, 1985; Millar, 1997; Hughes et al., 2010) and with data from the literature suggesting that the average speed for an expert blind reader is around $30 - 40 \pm 5$ mm/s (Hughes et al., 2010).

We will further investigate the neural coding issues addressed in this paper in order to better explore the role of (i) different types of CN receptive fields (i.e. kernel functions sampling the mechanoreceptor activity space), and (ii) possible spike-timing-dependent plasticity (STDP) mechanisms (Bi and Poo, 1999) to obtain optimal mechanoreceptor-to-CN synaptic weight distributions in a more biologically plausible manner. Also, we are currently implementing a closed-loop architecture—involving mechanoreceptors, CN neurones, a high level classification process and a cerebellar low-level controller—to study sensorimotor control in fine touch discrimination tasks (e.g. Braille reading).

Acknowledgements

This research was granted by the EC Project SENSOPAC (No. IST-027819-IP) and by the "Direction Générale de l'Armement" (DGA, coordinator Didier Bazalgette). The authors also thank the "Consorzio interuniversitario per le Applicazioni di Supercalcolo Per Università e Ricerca" (CASPUR Consortium, www.caspur.it) for providing the high performance computing facilities used for simulations.

References

Bi, G., Poo, M., 1999. Distributed synaptic modification in neural networks induced by patterned stimulation. Nature 401, 792–796.
Bologna, L.L., Brasselet, R., Maggiali, M., Arleo, A., 2010. Neuromimetic encoding/decoding of spatiotemporal spiking signals from an artificial touch sensor, Neural Networks (IJCNN), The 2010 International Joint Conference, pp.1–6, doi:10.1109/IJCNN.2010.5596851.
Brasselet, R., Johansson, R.S., Arleo, A., 2009. Optimal context separation of spiking haptic signals by second-order somatosensory neurons. In: Bengio, Y., et al. (Ed.), Advances in Neural Information Processing Systems, vol. 22, pp. 180–188.
Brasselet, R., Johansson, R.S., Arleo, A., 2011. Quantifying neurotransmission reliability through metrics-based information analysis. Neural Comput. 23 (4), 852–881.
Canedo, A., Mariño, J., Aguilar, J., 2000. Lemniscal recurrent and transcortical influences on cuneate neurons. Neuroscience 97, 317–334.
Cannata, G., Maggiali, M., Metta, G., Sandini, G., 2008. An embedded artificial skin for humanoid robots. In: Proc. IEEE International Conference on Multisensor Fusion and Integration for Intelligent Systems MFI 2008, pp. 434–438.
Chacron, M.J., Pakdaman, K., Longtin, A., 2003. Interspike interval correlations, memory, adaptation, and refractoriness in a leaky integrate-and-fire model with threshold fatigue. Neural Comput. 15, 253–278.
Gerstner, W., Kistler, W., 2002. Spiking Neuron Models. Cambridge University Press.
Hughes, B., Gemmert, A.W.A.V., Stelmach, G.E., 2010. Linguistic and perceptual-motor contributions to the kinematic properties of the braille reading finger. Hum. Movement Sci.. doi:10.1016/j.humov.2010.05.005.
Johansson, R.S., Birznieks, I., 2004. First spikes in ensembles of human tactile afferents code complex spatial fingertip events. Nat. Neurosci. 7, 170–177.
Johansson, R.S., Flanagan, J.R., 2009. Coding and use of tactile signals from the fingertips in object manipulation tasks. Nat. Rev. Neurosci. 10, 345–359.
Jones, E.G., 2000. Cortical and subcortical contributions to activity-dependent plasticity in primate somatosensory cortex. Annu. Rev. Neurosci. 23, 1–37.
Lapicque, L., 1907. Recherches quantitatives sur l'excitation électrique des nerfs traitée comme une polarisation. J. Phys. Pathol. Générale 9, 620–635.
Millar, S., 1997. Reading by Touch. Routledge, London, New York.
Mousty, P., 1985. A study of braille reading. I: Reading speed as a function of hand usage and context. Quart. J. Exp. Psychol. A 37, 217–233.
Phillips, J., Johansson, R., Johnson, K., 1990. Representation of braille characters in human nerve fibres. Exp. Brain Res. 81, 589–592.
Phillips, J.R., Johansson, R.S., Johnson, K.O., 1992. Responses of human mechanoreceptive afferents to embossed dot arrays scanned across fingerpad skin. J. Neurosci. 12, 827–839.
Rieke, F., Warland, D., de Ruyter van Stevenick, R., Bialek, W. (Eds.), 1997. Spikes: Exploring the Neural Code. MIT Press, Cambridge.
Sánchez, E., Barro, S., Mariño, J., Canedo, A., 2003. A computational model of cuneothalamic projection neurons. Network 14, 211–231.
Schreiber, S., Fellous, J.M., Whitmer, D., Tiesinga, P., Sejnowski, T.J., 2003. A new correlation-based measure of spike timing reliability. Neurocomputing, 925–931.
Shannon, E., 1948. A mathematical theory of communication. Bell Syst. Tech. J. 27, 379–423, 623–656.
Vallbo, A.B., Johansson, R.S., 1984. Properties of cutaneous mechanoreceptors in the human hand related to touch sensation. Hum. Neurobiol. 3, 314.
Van Rossum, M.C., 2001. A novel spike distance. Neural Comput. 13, 751–763.
Victor, J.D., Purpura, K.P., 1996. Nature and precision of temporal coding in visual cortex: a metric-space analysis. J. Neurophysiol. 76, 1310–1326.